Conference on Modelling Fluid Flow (CMFF'22)
The 18th International Conference on Fluid Flow Technologies
Budapest, Hungary, August 30-September 2, 2022

Can black blood MRI predict hemodynamics in intracranial aneurysms? - An analysis of in-vitro signal intensity and CFD

Jana KORTE[1,3], Laurel MARSH[2,3,4], Mariya PRAVDIVTSEVA[5], Franziska GAIDZIK[2,3], Naomi LARSEN[5], Gábor JANIGA[2,3], Philipp BERG[2,3],

[1] Corresponding Author. Department of Fluid Dynamics and Technical Flows, University of Magdeburg, Universitaetsplatz 2, 39106 Magdeburg, Germany, E-mail: jana.korte@ovgu.de
[2] Department of Fluid Dynamics and Technical Flows, University of Magdeburg, Magdeburg, Germany
[3] Research Campus STIMULATE, University of Magdeburg, Germany
[4] Department of Mechanical Engineering, University of Washington, Seattle, USA
[5] Department of Radiology and Neuroradiology, University Medical Center Schleswig-Holstein (UKSH), Kiel University, Kiel, Germany

ABSTRACT

By visualizing vascular walls of intracranial aneurysms (IA) using black blood magnetic resonance imaging (BB MRI), wall adjacent and luminal hyperintense signal intensity (SI) is found. These SI have been linked to vessel wall inflammation, higher rupture risk, and slow flow. However, the relationship between SI and other hemodynamic features has not been investigated before. Therefore, here computational fluid dynamics (CFD) simulations are carried out to compare the flow behaviour to the SI values. In this study, three patient-specific aneurysm phantoms are undergone BB MRI. Next BB MRI SI were evaluated inside the aneurysm lumen and is then compared to in-silico flow behaviour. The comparison is performed by taking both, the time-averaged (TA) and time-resolved CFD data into account. The overall comparison reveals high dependencies of increasing velocity and kinetic energy (KE) to decreasing SI, which can be explained by the design of BB MRI. BB MRI eliminate the signal of flowing fluid and works best for higher flows. Still, not all BB signal originated from fluid with high average velocities was eliminated, in this case it shows higher oscillatory velocity indices. By analysing regions of vortex formation within the highly-resolved CFD data, a correlation to low SI is found. The comparative investigation of BB and CFD results indicates specific relations between hemodynamics and SI noticeable in velocity, KE and vortex formation. The analysis of BB MRI SI reveals correspondences to hemodynamic parameters for TA values, a strong correlation has to be further proofed.

Keywords: Computational fluid dynamics, Black blood magnetic resonance imaging, Hemodynamics, Intracranial aneurysm

NOMENCLATURE

KE	$[J]$	kinetic energy
OVI	$[-]$	oscillatory velocity index
SI	$[a.u.]$	signal intensity
VEL	$[m/s]$	velocity

Subscripts and Superscripts

BB	black blood
CFD	computational fluid dynamics
IA	intracranial aneurysm
MAD	median absolute deviations
MRI	magnetic resonance imaging
TA	time average
VC	vortex core
VW	vessel wall

1. INTRODUCTION

Intracranial aneurysms (IAs) are a pathology occurring in cerebral arteries, presenting as a dilatation of the vessel [1]. Due to the weak structure of an aneurysm dome, IAs carry the risk of rupture which leads to subarachnoid bleedings. IAs can be treated, but each intervention has complication risk, moreover some IAs do not rupture during the lifetime. However, reliable aneurysm rupture risk assessment is a clinical challenge [2][3]. Many metrics associated with rupture risk can be derived from state-of-the-art CFD methods [4]. Specific hemodynamic parameters characterizing the blood flow are linked to rupture like oscillatory shear index and wall shear stress. Recently, signal enhancement on BB MRI was linked to the aneurysm wall inflammation and higher aneurysm rupture risk [5][6][7]. BB MRI recordings comprise of signal intensity and is designed to suppress the signal of flowing blood [8][9]. Low SI within measurements of IAs has been

related with high velocities. Nevertheless, recent studies show that low or high velocities can lead to low SI [8][10]. Overall the link between SI and aneurysm hemodynamics is of great interest concerning the estimation of rupture risks of IAs. Since this link was poorly investigated up to now, the purpose of this study is to determine relations of the intra-aneurysmal flow field to the BB SI. To explain the variations in SI trends and pseudo enhancement, the SI is compared to specific hemodynamic parameters.

2. MATERIAL AND METHODS

The underlying experiments and simulations are based on previous studies by Gaidzik et al. [10] and Pravdivsteva et al. [8].

2.1. Patient selection

Three IA models are created using 3D rotational angiography (3D RA, Allura XperFD 20/10, Philips, Best, The Netherlands) of three different patients over the age of 50. Each patient-specific IA model has a unique shape, size and location to ensure a diverse basis for the study. Size and shape of each model is shown in Figure 1 and are further described in [10][8].

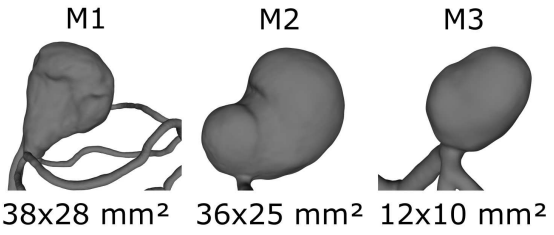

Figure 1. Aneurysm models (M1-3) of three different patients with varying anatomical cross sections (mm²) located at the basilar tip (M1), the carotid terminus (M2) and the middle cerebral artery bifurcation (M3).

2.2. Black blood MRI

Blood flow inside the IA models is analysed via in-vitro experiments of the patient-specific models. The IA geometry models are 3D-printed for this purpose and a blood mimicking fluid is pumped through the vessels with a pulsatile flow. Blood flow is then recorded with BB MRI. Within BB MRI the flowing blood is suppressed and enhancement zones further visualized. If the suppression sequencing is successful, blood is visualized as black (in contrast to this for in-vivo experiments the static tissue is illuminated). These visualizations are digitised to SI values, which are time averaged over one cardiac cycle. Resolution of the BB MRI voxel is 0.7mm³. For further details on the experimental setup the interested reader is referred to [8].

2.3. Hemodynamic simulations

For each model a blood-flow simulation is carried out based on the experimental setup to create a basis for comparison. The detailed setup is given in [10]. Fluid properties are set to equal the experimental parameters with a density of 1114.5 kg/m³ and a dynamic viscosity of 3.72 mPas, respectively. Time dependent pulsatile flow curves, recorded during the experiments, are set as inlet boundary conditions. Two different flow curves are imposed to analyse the impact of a high and low flow field. The mean value of the low flow curves are 160 ml/min (M1), 203 ml/min (M2) and 208 ml/min (M3). For the high flow curves, the mean values are 266 ml/min (M1), 307 ml/min (M2) and 311 ml/min (M3). Outlet boundary conditions are pressure curves, likewise recorded and set equal for high and low inflow conditions. The mesh comprises of polyhedral and prismatic cells with a base size is 0.1 mm and the discretised models comprised of 9.8 (M1), 15.1 (M2) and 8.5 (M3) million elements. The finite-volume solver used for the simulations is StarCCM+ (Siemens Product Lifecycle Management Software Inc., Plato, TX, USA).

2.4. Analysis

To compare the SI data recorded within the BB MRI experiments to the CFD data, relevant hemodynamic parameters are evaluated from the numerical simulations. Accordingly, velocity magnitude as well as velocity components (V_x, V_y, V_z), kinetic energy (KE), and oscillatory velocity index (OVI) are analysed [11][12].

$$KE = \frac{\rho v^2}{2} \tag{1}$$

$$OVI = \frac{1 - \frac{|\int_0^T f v_i dt|}{\int_0^T |f v_i| dt}}{2} \tag{2}$$

The qualitative as well as quantitative evaluation of the raw CFD data is carried out in EnSight v10.2 (ANSYS Inc., Canonsburg, PA, USA). MATLAB R2020b (MathWorks, USA) is used for the analysis of the processed data [13]. For an accurate comparison the BB SI data has to be registered onto the numerical model results. Registration is carried out in Blender 3.1 (Blender Foundation, Amsterdam, NL). Once this SI data is registered, the CFD data, whether time-averaged or resolved, can be mapped, using Ensight, onto the BB voxels to allow for direct comparison.

2.4.1. Time-averaged data analysis

After registration of the SI data onto the hemodynamic simulation parameters, the latter are averaged and mapped onto the registered SI data. Thus, a point-wise comparison of the averaged data is accomplished. Since the mapped, time-averaged (TA)

data still may be slightly misaligned, a voxel-wise comparison is completed as well. For this, the CFD data is spatially discretised and the averaged parameters are calculated for a new, artificial voxelisation. This new voxel size is 2.1mm³, which is three times the size of the BB MRI resolution. The spatially averaged CFD data are then similarly mapped onto the new SI data which is spatially averaged to the same resolution, to analyze the correlation of the data voxel-wise.

Additionally, the mapped SI data is clustered into 10 and 25 regions depending on the value of the SI. Thus, the cluster boundaries feature a regular interval and the dimensions of each cluster differs in size. The cluster-wise averages of the hemodynamic parameters depending on the SI values within each cluster, are then correlated to the cluster-wise SI values.

To define these clusters, the range of SI is divided in equal amounts between the minimum and maximum based on the number of regions. Thus, every cluster has a specific size and discretizing a model into more than 25 clusters would not improve the analysis since clusters become bare or completely void. On top of that, for the highly resolved CFD data, the OVI is calculated. Since this index shows the fluctuation of velocity over time, it is first calculated and then mapped onto the registered BB SI data. Here, a cluster-wise correlation allows for an analysis of the dependency of velocity fluctuations over time onto SI.

2.4.2. Time-resolved data analysis

To further investigate the fluxes of SI observable in the flow fields and possible causes of pseudo-enhancement, the time-resolved CFD data is analysed in detail and then mapped onto the BB SI. This analysis contains the evaluation of each time-step's velocity values. Focusing on the systolic time-step, the inflow jet into the aneurysm is evaluated and the depending velocity parameters are analysed.

Next, the dependencies between vortex formation and BB MRI are analysed. By extracting the vortex core (VC) lines from the high resolved CFD data, the geometric points of the inner vortex is formed. These are given over 20 time-steps within one cardiac cycle. After the vortex core region is located, the BB SI is analysed in this location. The variation of high and low BB SI and the mean and median values are analysed.

3. RESULTS

3.1. Qualitative results

Figure 2 shows the qualitative comparison of the three models. A contour inside each aneurysm model is colored by time-averaged KE (first and third row) and SI (second and forth row). Similar flow patterns are present within M1 and M2 for SI and KE for low and high flow rates, constituting the appearance of higher SI in areas with lower KE (see black arrow heads). This is also noticeable within M3 for the high flow rate (see black arrow heads). KE pattern is similar within M3 for low and high flow rate, but the SI pattern shows a different behaviour between low and high flow. Furthermore, SI is much lower (highest value 830 a.u. lower) within M3 for low flow.

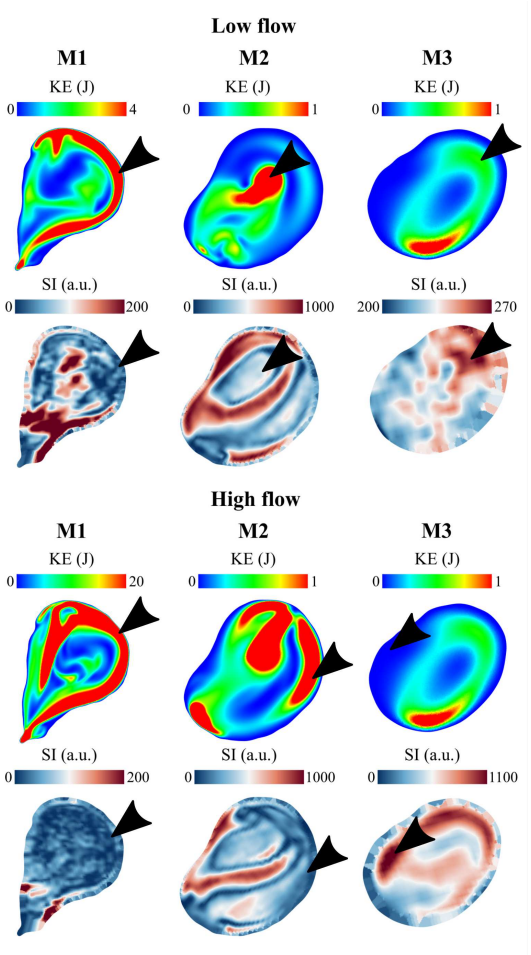

Figure 2. Contour through each aneurysm model (M1-M3) colored with KE (first and third row) and with SI (second and forth row) for the two applied flow rates. Areas with higher KE correlate with areas with lower SI and vice versa (black arrow heads).

3.2. Quantitative results

3.2.1. Time-averaged data

As previously reported, the mean TA velocity correlates to the inverse of the SI when clustering the domain into regions based on equivalent intervals of SI. Comparing the values point-wise and voxel-wise as described in section 2.4 does not give insight into the flow behaviour and its impact on the SI. Nevertheless, the cluster-wise comparison shows similarities between the BB MRI SI and other hemodynamic parameters. In Figure 3 the TA velocity is presented for each of the ten SI clusters. In this Figure as well as in Figure 4 and Figure 5 the SI values are nor-

malized by the highest SI value outside the aneurysm lumen. In the graph on the left, the TA velocity is plotted with all data points while the graph on the right shows the data with outlying velocity removed. Outliers are defined as points with more than three scaled median absolute deviations (MAD). Figure 3 shows the wide range of velocities that can induce low SI for M1. While high velocities are expected in the lower range of SI, a large percentage of the first two clusters show a vast range which includes very low velocity. After removing the outliers, the median shifts most noticeably for the first, second and third clusters. Considering only the velocities falling within three MAD of the median, shows that the last region's median velocity is similar to the results including the outliers. Therefore, further investigation

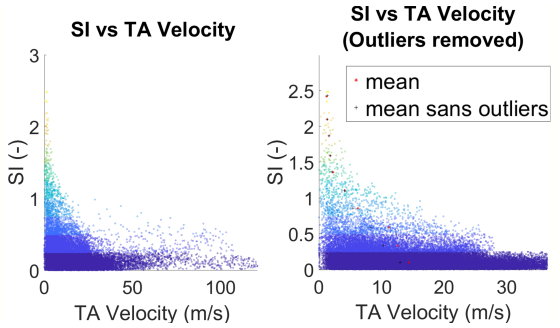

Figure 3. TA velocity (m/s) over the SI clusters (1-10) with (left) and without (right) outliers.

is performed to elucidate the correspondence of this large scale of velocities and SI.

3.2.2. Time-resolved data

Concerning the time-resolved CFD data, the systolic time step is analysed first. Here, the high velocity and the corresponding OVI are taken into account. The high velocity inflow of M1 at systolic state is shown in Figure 4 along with the OVI. In the first row, the velocity inflow jet is presented using only velocity above the 90th (left) and 99th (right) percentile of the overall velocity values. The jet is colored by velocity; the red dots are a subset of the CFD resolution thereby representing the aneurysm. In the second row, the jet is simply colored blue while the aneurysm representative dots are scaled and colored by OVI. The high velocity zone has a consistent direction throughout the cardiac cycle producing a low OVI. However, the fluid surrounding the jet changes direction throughout the cycle.

A high OVI (OVI > 0.2) is typically found in low velocity areas where relatively minor change in direction or particularly in magnitude can lead to an elevation of OVI. In Figure 5 the distribution of the OVI in the aneurysm lumen is presented on the left. In the middle, the aneurysm lumen is presented with blue dots. Using the first quartile of velocity as a limit, velocity in this range exhibits a high OVI over the entire range of SI as shown in Figure 5 in the

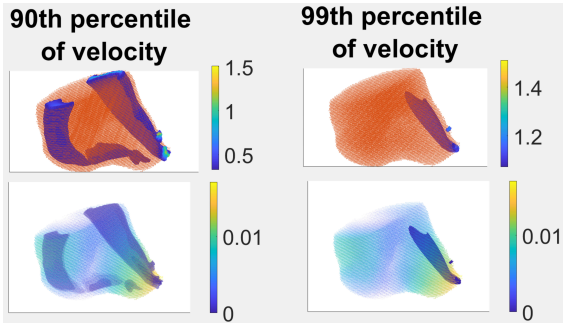

Figure 4. Velocity inflow jet into aneurysm M1 scaled by OVI inside the red colored aneurysm (first row) and the velocity inflow jet colored blue inside the aneurysm scaled with OVI (second row).

middle. However, for the fluid with velocity greater than the mean and OVI greater than 0.2, the SI tends to be in its higher range (see Figure 5 right). The

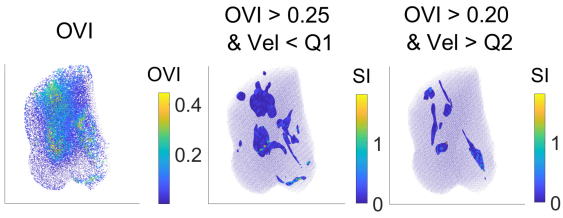

Figure 5. OVI distribution inside the aneurysm (left). Distribution of OVI>0.25 and velocity lower than the first cluster (middle). Distribution of OVI>0.2 and velocity higher than the second cluster (right).

relationship between TA velocity and SI does not hold for time-resolved velocities in most cases even at systole where the largest ranges of velocity would be seen. The M1 high flow case saw the largest velocities of the study. In Figure 6, the velocities of systolic flow are analysed in comparison to the averaged cardiac cycle. Here it is more apparent that a majority of flow, even at median velocities, is suppressed well in the first two regions. However, average velocity does not correlate with SI. A lack of any trend between velocity and SI is noted when the clustering is based on velocity.

Concerning the vortex core analysis, the SI, revealed in the vortex core regions, is analysed for each time-step. No specific curve representing a periodicity of the SI is found over time. Calculating the mean values of the SI of each time-steps reveals very low (<first cluster = 50 a.u.) SI values. In Figure 7 the mean and median as well as maximum and minimum values are shown. The maximum comprises of a high range ($\vec{\Delta}$230 a.u.) over SI, while the mean, median and minimum values range only up to 4 a.u..

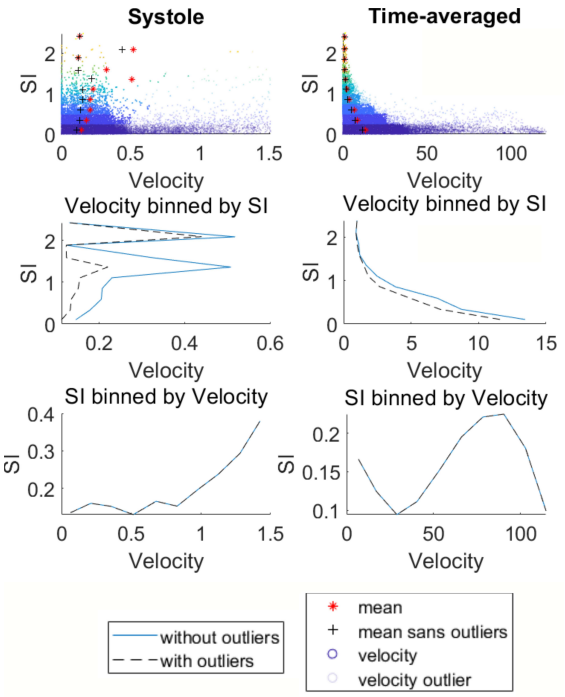

Figure 6. SI plotted over velocity in systolic state (left column) and TA (right column).

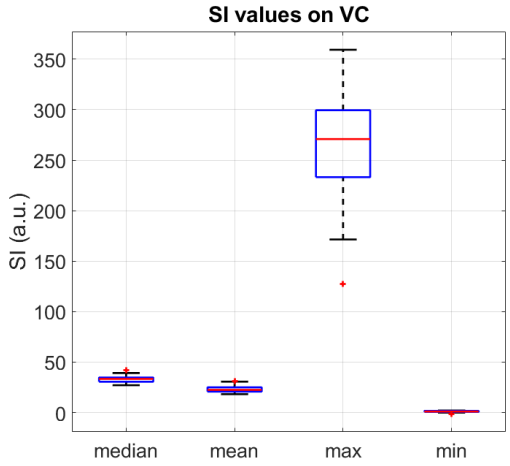

Figure 7. SI values on the VC of aneurysm M1, comprising the median, mean, maximum, and minimum values of SI for each time-step over one cardiac cycle.

4. DISCUSSION

Investigating the dependencies between SI and hemodynamics reveals a visible connection that with increasing kinetic energies the SI decreases. This strengthens the findings by [10] and [8]. A point-wise correlation, whether using highly-resolved or voxelised data, does not provide any clear correlation. For the high resolution data, this could be attributed to the manual registration and lower resolution of BB MRI. The artificial voxelisation provides an averaging effect that can obscure registration errors, but also erases important information like velocity component directions and peaks. Thus, still no direct relationship arose between the hemodynamics and SI, when analysing spatial averages. Dividing the SI data into 10 clusters reveals a correlation to TA velocity. The analysis of the time-resolved data is narrowed down by focusing on systole and diastole along with OVI, a metric summarising the entire cardiac cycle. There is no specific correlation found for the time-resolved data. Since the SI data is inherently time-averaged itself, this may mean that only time-averaged data is able to be infered. Similarly and more surprisingly, time-averaged data may be the only way of determining why enhancement and other artifacts arise in BB MRI. This leads to the assumption that SI data correlates solely to TA hemodynamics. Velocities greater than the first quartile of values is much less likely to have an OVI > 0.2; however, when these velocities, particularly when greater than the mean, experience high OVI, the flow exhibits a higher SI. This indicates that higher average velocities that are not consistently suppressed are yielding a higher SI due to an elevated OVI. This corresponds with Henningson et al., who found out that the signal suppression is more successful when a stronger turbulence appears [14]. A relationship is found for the TA data, but does vary between models. A larger number of models must be analysed to further strengthen the study.

5. CONCLUSION

In this study, three IA models are analysed with BB MRI and CFD to investigate their correlation. Therefore, the correlation between hemodynamic parameters calculated in CFD are linked to SI measured in VW MRI to investigate any possible correspondence. In summary, a qualitative and quantitative relation is clear for TA data. However, point-wise comparison as well as spatial discretization reveals no fertile insights. Especially when analysing the time-resolved CFD data separately, low OVI values paired with high velocities lead to better signal suppression (low SI). Vortex core lines are also correlated with low SI. All in all, a relation is found for BB MRI SI and TA hemodynamic parameters, showing lower velocity values with higher SI values.

ACKNOWLEDGEMENTS

This study was funded by the Federal Ministry of Education and Research within the research campus STIMULATE (grant number13GW0473A). The authors are grateful for the financial and intellectual support by the Research Training Group “Materials4Brain” (GRK2154; P2) and the European Structural and Investment Funds (ZS/2016/08/80646). Further support by the cluster of excellence Precision Medicine in Inflammation PMI 1267 and the faculty of medicine for funding the core facility MOIN CC is acknowledged. Furthermore, the financial sup-

port of the DFG (Deutsche Forschungsgemeinschaft) for Jana Korte within the project SPP2311 “Robust Coupling of Continuum-biomechanical In Silico Models to Establish Active Biological System Models for Later Use in Clinical Applications – Co-design of Modelling, Numerics and Usability” (project number 441884911) is gratefully acknowledged.

REFERENCES

[1] Cebral, J. R., Castro, M. A., Burgess, J. E., Pergolizzi, R. S., Sheridan, M. J., and Putman, C. M., 2005, “Characterization of cerebral aneurysms for assessing risk of rupture by using patient-specific computational hemodynamics models”, *AJNR: American Journal of Neuroradiology*, Vol. 26 (10), pp. 2550–2559.

[2] Kaminogo, M., Yonekura, M., and Shibata, S., 2003, “Incidence and outcome of multiple intracranial aneurysms in a defined population”, *Stroke*, Vol. 34 (1), pp. 16–21.

[3] Winn, H. R., Jane, J. A., Taylor, J., Kaiser, D., and Britz, G. W., 2002, “Prevalence of asymptomatic incidental aneurysms: review of 4568 arteriograms”, *Journal of neurosurgery*, Vol. 96 (1), pp. 43–49.

[4] Qian, Y., Takao, H., Umezu, M., and Murayama, Y., 2011, “Risk analysis of unruptured aneurysms using computational fluid dynamics technology: preliminary results”, *AJNR: American Journal of Neuroradiology*, Vol. 32 (10), pp. 1948–1955.

[5] Larsen, N., Flüh, C., Saalfeld, S., Voß, S., Hille, G., Trick, D., Wodarg, F., Synowitz, M., Jansen, O., and Berg, P., 2020, “Multimodal validation of focal enhancement in intracranial aneurysms as a surrogate marker for aneurysm instability”, *Neuroradiology*, Vol. 62 (12), pp. 1627–1635.

[6] Edjlali, M., Guédon, A., Ben Hassen, W., Boulouis, G., Benzakoun, J., Rodriguez-Régent, C., Trystram, D., Nataf, F., Meder, J.-F., Turski, P., Oppenheim, C., and Naggara, O., 2018, “Circumferential Thick Enhancement at Vessel Wall MRI Has High Specificity for Intracranial Aneurysm Instability”, *Radiology*, Vol. 289 (1), pp. 181–187.

[7] Quan, K., Song, J., Yang, Z., Wang, D., An, Q., Huang, L., Liu, P., Li, P., Tian, Y., Zhou, L., and Zhu, W., 2019, “Validation of wall enhancement as a new imaging biomarker of unruptured cerebral aneurysm”, *Stroke*, Vol. 50 (6), pp. 1570–1573.

[8] Pravdivtseva, M. S., Gaidzik, F., Berg, P., Hoffman, C., Rivera-Rivera, L. A., Medero, R., Bodart, L., Roldan-Alzate, A., Speidel, M. A., Johnson, K. M., Wieben, O., Jansen, O., Hövener, J.-B., and Larsen, N., 2021, “Pseudo-enhancement in intracranial aneurysms on black-blood MRI: Effects of flow rate, spatial resolution, and additional flow suppression”, *Journal of Magnetic Resonance Imaging : JMRI*.

[9] Mandell, D. M., Mossa-Basha, M., Qiao, Y., Hess, C. P., Hui, F., Matouk, C., Johnson, M. H., Daemen, M. J. A. P., Vossough, A., Edjlali, M., Saloner, D., Ansari, S. A., Wasserman, B. A., and Mikulis, D. J., 2017, “Intracranial vessel wall MRI: Principles and expert consensus recommendations of the american society of neuroradiology”, *AJNR: American Journal of Neuroradiology*, Vol. 38 (2), pp. 218–229.

[10] Gaidzik, F., Pravdivtseva, M., Larsen, N., Jansen, O., Hövener, J.-B., and Berg, P., 2021, “Luminal enhancement in intracranial aneurysms: fact or feature?-A quantitative multimodal flow analysis”, *International Journal of Computer Assisted Radiology and Surgery*, Vol. 16 (11), pp. 1999–2008.

[11] Mut, F., Löhner, R., Chien, A., Tateshima, S., Viñuela, F., Putman, C., and Cebral, J., 2011, “Computational hemodynamics framework for the analysis of cerebral aneurysms”, *International Journal for Numerical Methods in Biomedical Engineering*, Vol. 27 (6), pp. 822–839.

[12] Sano, T., Ishida, F., Tsuji, M., Furukawa, K., Shimosaka, S., and Suzuki, H., 2017, “Hemodynamic differences between ruptured and unruptured cerebral aneurysms simultaneously existing in the same location: 2 case reports and proposal of a novel parameter oscillatory velocity index”, *World neurosurgery*, Vol. 98, pp. 868.e5–868.e10.

[13] Korte, J., Marsh, L., Gaidzik, F., Pravdivtseva, M., Larsen, N., and Berg, P., 2021, “Correlation of black blood MRI with image-based blood flow simulations in intracranial aneurysms”, *Current Directions in Biomedical Engineering*, Vol. 7 (2), pp. 895–898.

[14] Henningsson, M., Malik, S., Botnar, R., Castellanos, D., Hussain, T., and Leiner, T., 2022, “Black-blood contrast in cardiovascular MRI”, *Journal of magnetic resonance imaging : JMRI*, Vol. 55 (1), pp. 61–80.